Available online at www.sciencedirect.com
SCIENCE DIRECT®
Journal of Sound and Vibration 274 (2004) 249–271
JOURNAL OF SOUND AND VIBRATION
www.elsevier.com/locate/jsvi

Multichannel active noise control system for local spectral reshaping of multifrequency noise

M. de Diego*, A. Gonzalez, M. Ferrer, G. Piñero

Dept. of Comunicaciones, Universidad Politecnica de Valencia, Camino de Vera s/n, Valencia 46022, Spain

Received 10 October 2002; accepted 20 May 2003

Abstract

This paper discusses the development of a multichannel active system for local spectral reshaping of multitone noise. The aim of this work is to design a real practical system that performs well in local active noise control (ANC) applications, and so improving the comfort sensation produced by enclosed sound fields. The adaptive algorithm implemented in the controller is a multichannel extension of the multifrequency adaptive equalizer developed by Kuo. The philosophy behind these equalizers lies in independently controlling some given frequencies of a primary signal. Moreover, the algorithm should manage to generate usefully sized zones of equalization in order to allow for the head motion of somebody with restricted mobility; for example, a passenger seated in a car. To verify the successful implementation of the multichannel system, experiments were carried out under listening room conditions. The developed prototype consists of an array of up to four microphones used as error sensors and two secondary sources. A 4100-type *Bruel and Kjaer* mannequin with two calibrated microphones at the ear canals was used to measure sound levels in a hypothetical listener's head. Different synthesized repetitive noises were used, as reference signals, specifically repetitive noise with harmonics of 15, 20, and 28 Hz, as well as an 80 Hz single tone. The equalized points include an area around the error sensor positions, and these are measured using the mannequin and an x–y moving platform. The extent to which the experimental equalization zones obtained favourable results validates the multichannel local ANC equalization system. Different error sensor positions around the listener head were also tested. The residual field inside the equalization zone was measured in all cases.

*Corresponding author. Tel.: +34-96-3879763; fax: +34-96-3877309.
E-mail address: mdediego@dcom.upv.es (M. de Diego).

0022-460X/$ - see front matter © 2003 Elsevier Ltd. All rights reserved.
doi:10.1016/j.jsv.2003.05.009

1. Introduction

Advances in digital signal processing and the versatility of active control techniques have enabled the development of new applications using active noise control (ANC) techniques. Traditionally, in an ANC system, the pressure signal at some cancellation microphones, called error signals, is cancelled out by the action of secondary sources that create a quiet zone around these points. Nowadays, new applications can be considered that take into account the subjective impression that active control produces on listeners. Active controllers designed for these applications should be capable of creating a given residual field around the head of the listener. In this direction a broadband active noise compressor was developed by Feng et al. [1,2] that can automatically adjust the residual noise power to a desired range. In some cases, the consideration of the psychoacoustical sensation caused by noise determines the need to retain some residual noise [3,4] in order to create a specific acoustic field. Instead of cancellation of sounds it is desirable to reshape some frequency components; for example, inside a car, it would be useful to keep some audible information from the engine to improve safety or to feel more comfortable. Although this can be difficult to achieve since people perceive acoustic comfort in different ways, some meaningful results have already been obtained [4,5]. This paper is focused on shaping interior repetitive noise, through the development of active noise equalizers (ANEs). The objective of this paper is to develop a real multichannel active noise equalization system that manages to independently amplify, or attenuate, selected frequencies of the primary signal in order to reshape the sound field in a meaningful controlled spatial zone. This system has become a valuable tool to improve the subjective perception of sounds [5].

ANE systems arose from traditional adaptive noise cancellers applied to repetitive noise. A single frequency adaptive noise canceller was initially proposed by Widrow et al. [6] and extended to the multifrequency case by Glover [7]. Thanks to the use of a two-weight adaptive filter for each of the reference signal frequencies, the system can adaptively adjust the amplitude of the unwanted noise. When the frequency of the periodic noise is known, or is obtained from a non-acoustic sensor such as a tachometer on a rotating machine, the adaptive noise canceller can internally generate a sinusoid as the reference signal [8].

The filtered-X LMS algorithm [9] (FXLMS) and its multichannel version, the multiple error LMS algorithm [10] (MELMS), are the most widely used adaptive filtering strategies applied to single or multiple channel adaptive noise cancellers for narrowband ANC applications [11]. For periodic signals, these algorithms become adaptive notch filters that remove the most powerful spectral components of the primary signal. The stability of adaptive notch filters using the FXLMS algorithm has been analyzed in Refs. [12,13]. Nevertheless, narrowband noise can only be attenuated using these algorithms. To reshape the sound field, ANEs should be alternatively considered.

A single frequency active noise equalizer (SFANE) was proposed in Refs. [14,15] that used the FXLMS algorithm to adapt the coefficients of a two-weight filter minimizing a pseudo-error signal instead of the residual noise. The SFANE was also configured in parallel to shape the residual noise spectrum. This active harmonic noise equalizer system had M single frequency ANEs to deal with the harmonic noises, and it was implemented on a real PVC duct. The multichannel extension of these ANEs is developed in this paper. Firstly, the algorithms implemented in the controller are analyzed, all of them being derived from traditional ANC

algorithms. Then, the application of the multifrequency ANE in a real-time multichannel system is investigated by means of analytical results and laboratory experiments. The practical system implemented was mounted inside a wooden listening room (1.8 m × 2.3 m × 2.4 m). Two loudspeakers were used as control sources and up to four microphones acted as error sensors (2:2 or 2:4 systems). Different synthesized noises were used as reference signals; specifically, repetitive noise with harmonics of 15, 20, and 28 Hz, as well as a single 80 Hz tone.

The ability of the local ANC system to reshape the acoustic field depending on the parameters setting is examined. A 4100-type *Bruel and Kjaer* mannequin with two calibrated microphones at the ear canals was positioned close to the error sensors inside the listening room in order to record the different noise signals in a hypothetical listener's head with, and without, the application of ANC techniques. The active system should provide usefully sized zones of equalization in order to allow for the head motion of somebody with restricted mobility, for example a passenger seated in a car. With this aim, the head and torso mannequin was moved using a linear (x–y) movement platform with two step-by-step engines in order to measure the residual noise levels in the area where the local control system was controlling the acoustic field. Experimental verification tests with different parameters settings validate the use of the controller. Results show, with a suitable parameters setting, that the system is able to reshape the acoustic field around the error sensors and also that the equalization zones are large enough to allow the seated person to slightly move his, or her, head without significant performance degradation.

This paper is organized as follows. In Section 2 the different equalizer algorithms (the single channel FXLMS active noise equalizer described in Refs. [3,16] and its proposed multichannel version) are discussed. The local ANE prototype is described in Section 3, and finally, the experimental results are reported in Section 4.

2. Active noise equalization algorithms

The most widely used adaptive filtering strategies applied to ANC systems are the FXLMS [9], and its multichannel version, the multiple error LMS algorithm [10]. These are based on the LMS algorithm [17] minimizing the instantaneous error signal power. To actively control periodic signals Kuo et al. [3,14–16] proposed single and multifrequency ANEs, which minimize a pseudo-error signal instead of the residual error. These equalizers use the FXLMS algorithm to adapt the coefficients of two-weight filters, one for each reference signal (single tone). In Ref. [18], the multichannel version of the multifrequency ANE was discussed and then retermed multichannel ANE. It uses the multiple error LMS algorithm to adapt the filters' coefficients.

In this paper, the SFANE is initially described, then the multifrequency ANE algorithm and the multichannel extension of both ANEs are presented. The aim is to develop the extension of the ANE to a multichannel system so that it becomes more suitable for local control applications.

2.1. SFANE

Fig. 1 shows the block diagram of the SFANE modified for active control applications with the FXLMS algorithm [3,16]. The output of the two-weight filter, $y[n]$, is split into two branches, the

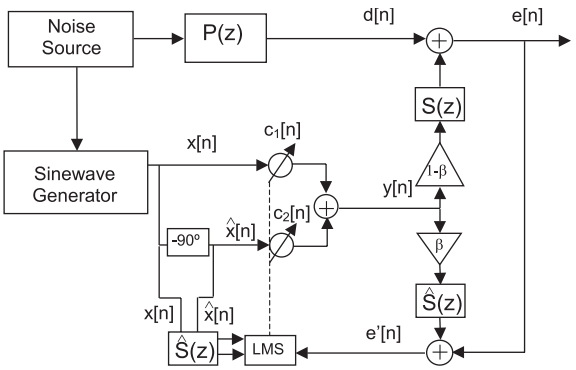

Fig. 1. Block diagram of the SFANE for active control applications.

balancing branch and the cancelling branch, and multiplied by gain parameter β and $(1-\beta)$, respectively.

A single cosine-wave generator was used to generate a reference input $x[n]$. The reference signal is assumed to be

$$x[n] = A\cos(\omega_0 n + \phi_0), \tag{1}$$

A and ϕ_0 being the amplitude and phase, respectively, of the normalized frequency signal and $\omega_0 = 2\pi/N$ its frequency, where N is an integer number.

The quadrature reference signal is derived from the reference signal with a 90° phase shift

$$\hat{x}[n] = A\sin(w_0 n + \phi_0). \tag{2}$$

The reference inputs feed a two-coefficients linear combiner to produce the cancelling signal, $y[n]$,

$$y[n] = c_1[n]x[n] + c_2[n]\hat{x}[n] = \mathbf{c}[n]^{\mathrm{T}}\mathbf{x}[n], \tag{3}$$

where $c_1[n]$ and $c_2[n]$ are the combiner weights. The input signal vector and the combiner coefficients vector at time n are given by

$$\mathbf{x}[n] = [x[n] \quad \hat{x}[n]]^{\mathrm{T}}, \tag{4}$$

$$\mathbf{c}[n] = [c_1[n] \quad c_2[n]]^{\mathrm{T}}. \tag{5}$$

Assuming that the adaptive filter intends to minimize the instantaneous power of a pseudo-error signal using the FXLMS algorithm, both weights are updated as [16]

$$\mathbf{c}[n+1] = \mathbf{c}[n] - 2\mu e'[n]\mathbf{x}'[n], \tag{6}$$

where $\mathbf{x}'[n]$ is a filtered version of the reference input vector. Thus

$$\mathbf{x}'[n] = [x'[n] \quad \hat{x}'[n]]^{\mathrm{T}} \tag{7}$$

and

$$x'[n] = \sum_{i=0}^{I-1} \hat{s}_i x[n-i],$$

$$\hat{x}'[n] = \sum_{i=0}^{I-1} \hat{s}_i \hat{x}[n-i]. \tag{8}$$

In Eq. (6), $e'[n]$, is the pseudo-error signal, and $\hat{s}_i$ is the ith coefficient of the secondary path estimated filter $\hat{S}(z)$. The filtered reference input vector can be expressed for mathematical convenience as $\mathbf{x}'[n] = \mathbf{x}[n]*\hat{s}[n]$, where $*$ denotes linear convolution and $\hat{s}[n]$ is the impulse response of the secondary path filter estimate $\hat{S}(z)$.

From Eqs. (1), (2), and (8), and knowing the reference signal frequency ω_0, the filtered reference signals can be expressed as

$$x'[n] = A\hat{A}_s \cos(\omega_0 n + \hat{\phi}_s) \tag{9}$$

and

$$\hat{x}'[n] = A\hat{A}_s \sin(\omega_0 n + \hat{\phi}_s), \tag{10}$$

$\hat{\phi}_s$ being the relative phase of $x'[n]$ with respect to $x[n]$, and $\hat{A}_s$ is the amplitude response of $\hat{s}[n]$ at frequency ω_0.

The error signal can be expressed as

$$e[n] = d[n] + (1-\beta)y[n]*s[n] \tag{11}$$

and the pseudo-error signal used in Eq. (6) as

$$e'[n] = e[n] + \beta y[n]*\hat{s}[n]. \tag{12}$$

Parameter β is termed the gain parameter at frequency ω_0 and its value determines the attenuation, or amplification, of the primary signal at the frequency achieved by the ANE. Four different work modes for actively controlling the primary signal at frequency ω_0 exist. They depend on β parameter values, when $S(z) = \hat{S}(z)$ for $z = e^{j\omega_0}$: $\beta = 0$ indicates cancellation mode, $0 < \beta < 1$ indicates attenuation mode, $\beta = 1$ keeps the signal intact, and $\beta > 1$ amplifies the signal by β.

Exploration of Fig. 1 and Eq. (12) shows that when $\hat{s}[n] = s[n]$ (perfect secondary path estimation) the pseudo-error can be expressed as [3]

$$e'[n] = d[n] + y[n]*s[n]. \tag{13}$$

After the filter convergence, according to Eq. (6) the pseudo-error signal becomes $e'[n] \approx 0$ and consequently from Eq. (13) the error signal, Eq. (11), at the reference frequency ω_0 can be rewritten as

$$e[n] \approx -\beta y[n]*s[n] \approx \beta d[n]. \tag{14}$$

For this reason, the output signal of the system, $e[n]$, contains a residue of the primary signal at frequency ω_0, adjustable by the gain parameter β.

2.2. Multiple frequency ANE

The multifrequency ANE, which enables control of K different frequency reference signals, is developed from K SFANE with FXLMS [14,16].

Fig. 2 shows the corresponding block diagram.

The kth ($k = 1, \ldots, K$) reference signal and its version filtered by the secondary path are

$$x_k[n] = A_k \cos \omega_k n \tag{15}$$

and

$$x'_k[n] = A_k \hat{A}_{sk} \cos(\omega_k n + \hat{\phi}_{sk}), \tag{16}$$

where $\hat{A}_{sk}$ and $\hat{\phi}_{sk}$ are the amplitude and phase, respectively, of $\hat{S}(z)$ to the kth normalized frequency ω_k (usually $\omega_k = (2\pi/N)k$, where N is an integer and $k < N$).

The input vector for the kth reference signal at time n is

$$\mathbf{x}_k[n] = [x_k[n] \quad \hat{x}_k[n]]^{\mathrm{T}}, \tag{17}$$

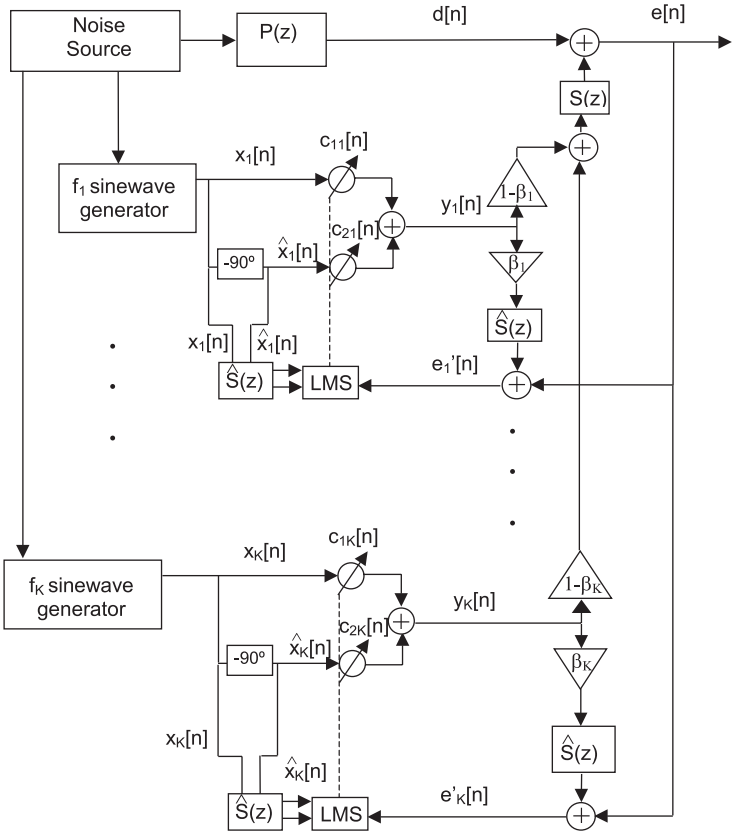

Fig. 2. Block diagram of the multifrequency ANE.

and the input vector of the kth reference signal at time n filtered by the secondary path estimation $\hat{s}[n]$ is

$$\mathbf{x}'_k[n] = [x'_k[n] \quad \hat{x}'_k[n]]^{\mathrm{T}}. \tag{18}$$

The error sensor signal is given by

$$e[n] = d[n] + \sum_{k=1}^{K} (1 - \beta_k) y_k[n] * s[n] \tag{19}$$

and the kth pseudo-error signal

$$e'_k[n] = e[n] + \beta_k y_k[n] * \hat{s}[n], \quad k = 1, \ldots, K, \tag{20}$$

where $y_k[n] = \mathbf{c}_k[n]^{\mathrm{T}} \mathbf{x}_k[n]$.

The different gain parameters to control for each frequency can be included in the following vector: $\mathbf{B} = [\beta_1, \ldots, \beta_K]^{\mathrm{T}}$.

There will be a two-coefficient adaptive filter, $\mathbf{c}_k[n]$, for each tone component of the reference signal and the FXLMS algorithm for the kth filter is

$$\mathbf{c}_k[n+1] = \mathbf{c}_k[n] - 2\mu e'_k[n] \mathbf{x}'_k[n]. \tag{21}$$

2.3. Multichannel ANE

The application of the ANE developed by Kuo et al., and described in Refs. [3,14–16] for active control applications, allows the sound field to be reshaped, thus adjusting independently the amplitude levels of each frequency forming the narrowband noise. However, the algorithm description is provided only for the control of harmonics in a single channel system, with a single error sensor, and a single secondary cancellation source.

It is difficult to achieve meaningful results in an enclosure using a single channel local ANC system because a single secondary source interacting with the system under control is unsuitable for exciting all modes of the primary acoustic field [19]. More than one error sensor is needed to enlarge the zone of controlled points belonging to the real space. In the final analysis, the use of several sources and error sensors avoids these problems by introducing some degree of spatial diversity, but the system grows in complexity with regard to its software requirements, analysis, and design. In practical applications, a multichannel ANE is required to equalize multiple narrowband components at the fundamental frequency and harmonics of the primary noise. As can be seen below, the single channel ANE is extended to the multiple channel algorithm for active noise equalization which is more suitable for local control; see Ref. [18] for an introduction to multichannel ANEs.

Consider a narrowband multichannel system (see Fig. 3) consisting of M secondary sources, L error sensors, and K reference signals [20,21], based on the feedforward multichannel system described by Elliott et al. [10]. The set of reference signals is usually provided by a synchronization signal, with the aim of controlling K harmonics generated as in Eq. (15).

The kth reference signal filtered by the secondary path estimation $s_{lm}[n]$ between the mth secondary source and the lth error sensor is

$$x'_{klm}[n] = A_k \hat{A}_{sklm} \cos(\omega_k n + \hat{\phi}_{sklm}), \tag{22}$$

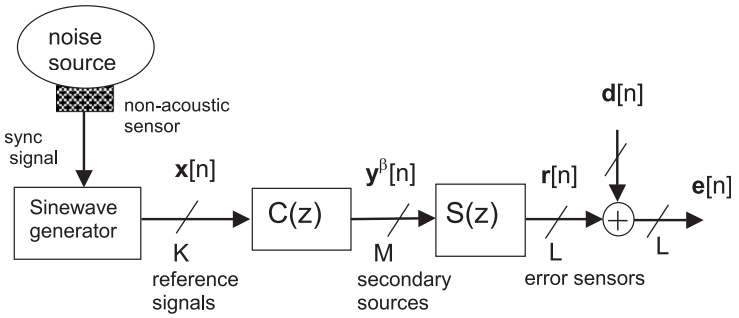

Fig. 3. Multichannel narrowband feedforward active noise equalization system.

$\hat{A}_{sklm}$ and $\hat{\phi}_{sklm}$ being the amplitude and phase, respectively, of the filter $\hat{S}_{lm}(z)$ at the kth normalized frequency ω_k.

The kth reference vector at time n filtered by the estimation of the secondary path, $s_{lm}[n]$, is

$$\mathbf{x}'_{klm}[n] = [x'_{klm}[n] \quad \hat{x}'_{klm}[n]]^{\mathrm{T}}. \tag{23}$$

The error signal at time n may be expressed as

$$e_l[n] = d_l[n] + \sum_{m=1}^{M} y_m^{\beta}[n] * s_{lm}[n], \quad l = 1, \ldots, L, \tag{24}$$

where $e_l[n]$ denotes the lth residual error, $d_l[n]$ is the primary signal at the lth error sensor, and $y_m^{\beta}[n]$ is defined as

$$y_m^{\beta}[n] = \sum_{k=1}^{K} (1 - \beta_k) y_{mk}[n], \tag{25}$$

$y_{mk}[n]$ being the output of the mth filter with a kth input signal.

The kth pseudo-error signal becomes

$$e'_{kl}[n] = e_l[n] + \beta_k \sum_{m=1}^{M} y_{mk}[n] * \hat{s}_{lm}[n], \quad l = 1, \ldots, L, \tag{26}$$

where β_k is the gain parameter which fixes the kth residual noise amplitude, and $\hat{s}_{lm}[n]$ is the estimation of the impulse response $s_{lm}[n]$.

There are M two-weight filters for each reference signal. For the kth reference signal, the updating coefficients take the usual form

$$\mathbf{c}_{km}[n+1] = \mathbf{c}_{km}[n] - 2\mu_k \sum_{l=1}^{L} e'_{kl}[n] \mathbf{x}'_{klm}[n], \tag{27}$$

where the corresponding weight vector is

$$\mathbf{c}_{km}[n] = [c_{1km}[n] \quad c_{2km}[n]]^{\mathrm{T}}. \tag{28}$$

The signal $y_{mk}[n]$ is generated by filtering the reference signal $\mathbf{x}_k[n]$ through the corresponding adaptive filter, $\mathbf{c}_{km}[n]$,

$$y_{mk}[n] = \mathbf{c}_{km}[n]^{\mathrm{T}}\mathbf{x}_k[n]. \tag{29}$$

A theoretical convergence analysis of the algorithm can be found in Ref. [22].

3. System description

The ANC was installed inside a rectangular enclosure. The enclosure interior was equipped to achieve the appropriate listening characteristics: acoustic insulation so that measurements could be performed without being affected by outside noises, as well as a suitable reverberation time which provides shorter impulse responses and more realistic conditions avoiding strong resonances.

As can be seen in Fig. 4, the active controller consists of a microphone array, also called error sensors, placed in positions chosen to monitor the desired controlled area. In addition to the microphones, a number of cancellation sources or secondary loudspeakers, and a primary loudspeaker, or primary noise source, are used.

The detailed description of the system is structured into several sections, first the acoustic characteristics of the room are described, then the electroacoustic system used will be explained, and finally, the measurement system will be described.

3.1. Acoustic characteristics of the room

The enclosure is a rectangular room made of chipboard measuring 1.80 m wide, 2.30 m long, and 2.40 m high. The geometry of the room gives frequency responses with strong resonances that depend on the dimensions of the room. The corresponding resonant frequencies [23], as well as their corresponding propagation modes, are shown in Table 1.

To shorten the impulse responses, several absorbing layers have been added, since these reduce part of the reflections of the acoustic signals off the walls. Finally, the enclosure ceiling has been

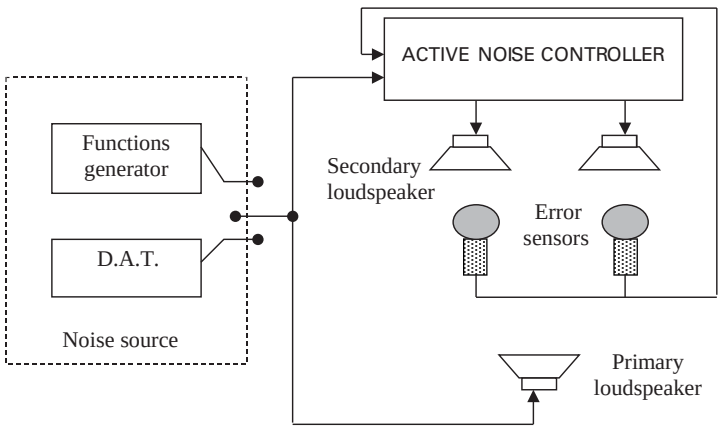

Fig. 4. Prototype of active noise equalization.

Table 1
First resonant frequencies

Room modes							
l	*m*	*n*	Frequency (Hz)	*l*	*m*	*n*	Frequency (Hz)
0	0	1	86.61	1	0	0	91.17
0	1	0	123.73	1	0	1	125.75
0	1	1	151.03	1	1	0	153.69
0	0	2	173.23	1	1	1	176.42
2	0	0	182.34	1	0	2	195.75
2	0	1	201.87	0	1	2	212.88
2	1	0	220.36	1	1	2	231.58
2	1	1	236.77	0	2	0	247.46
2	0	2	251.51	0	0	3	259.84
0	2	1	262.19	1	2	0	263.72

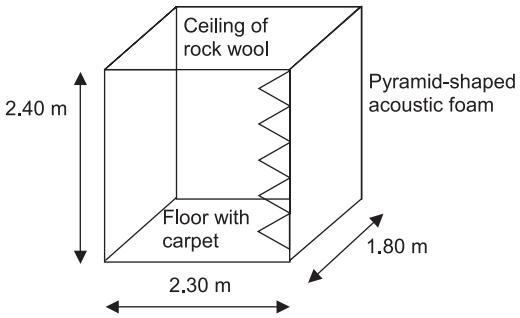

Fig. 5. Sketch of the listening room.

covered with rock wool and sack cloth, the floor carpeted, and the wall immediately opposite the primary noise source covered with pyramid-shaped acoustic foam. Fig. 5 shows a sketch of the equipped enclosure and Fig. 6 shows an example of the impulse and frequency responses of the conditioned listening room. It can be seen that the frequency response peaks match the resonant frequencies previously calculated.

3.2. *Electroacoustic system*

The multichannel system used consists of two secondary loudspeakers, and up to four error sensors. Fig. 7 illustrates the relative position of transducers inside the room. Loudspeakers are placed facing the mannequin, the secondary sources on each side of the primary source. The error sensors are located at different z planes. An array of up to four electret microphones were used as error sensors. The power supply for the electret microphones was supplied through a five-channel amplifier. The frequency response of the loudspeakers in the band studied could be considered flat, and with a fairly linear behaviour. The signals sent to the loudspeakers were previously amplified by the two audio amplifiers, working in the 20 Hz to 20 kHz band.

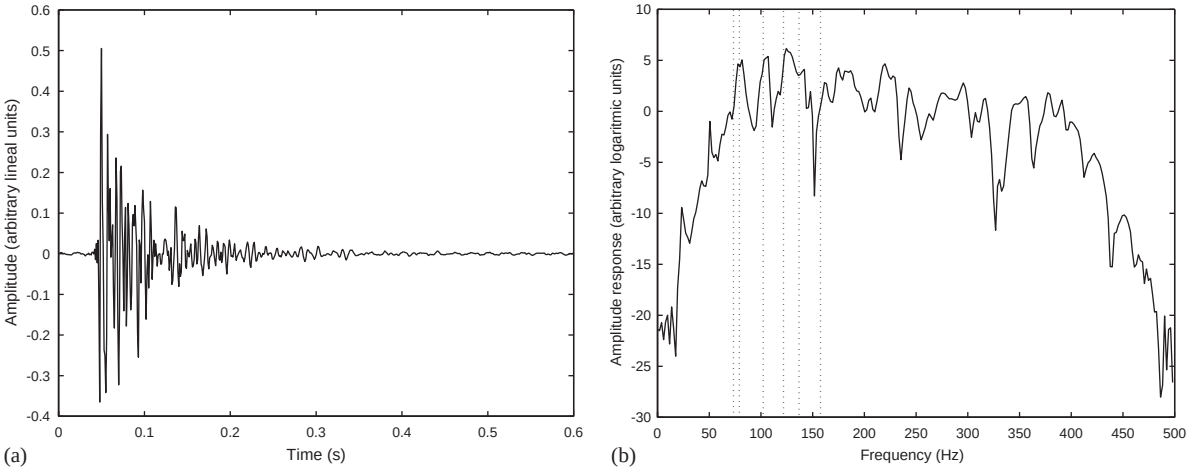

Fig. 6. (a) Impulse response and (b) amplitude of the frequency response of the listening room (dashed lines show first resonant frequencies).

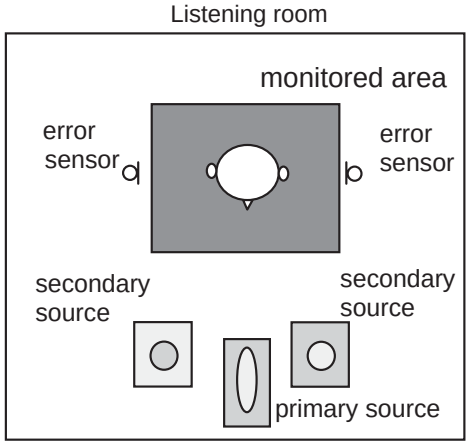

Fig. 7. Relative position of transducers inside the room.

A low-pass filtering of the signals coming from the error sensors was performed to avoid aliasing. This filtering was performed through linear phase FIR digital filters with 251 coefficients. The most frequently used filters have 230 Hz cutoff frequencies, sufficient to sample signals at 500 Hz. The reconstruction or interpolation filters were identical to those previously described, but in this case, they provide the appropriate signals after the digital/analogue conversion. All the algorithms were programmed in a Fulcrum board, using the TMS320C40 digital signal processor.

3.3. Description of the spatial measurement system

A system that enables measurement of the acoustic field in several points of the space in the intended control area is required to evaluate the active control system performance. By using this

measurement system a two-dimensional spatial distribution of sound levels at the listeners ears can be obtained.

As a first approach, one might consider taking simultaneous measurements at different points, or at successive time instants, while maintaining the measurement conditions invariable. This is difficult because as many measurement sensors as measurement points cannot usually be assumed. They should, at least, be moved inside the desired control area in order to carry out the spatial sampling. However there is a meaningful factor that should be taken into account in order to understand why the measurements were carried out in another way, namely, the acoustic sensation a listener experiences at different points within the controlled area. For this purpose, a 4100-type *Bruel* and *Kjaer* mannequin was used that emulates a human head and torso in terms of surface reflection and diffraction. However, mannequin displacement is a difficult task which can suffer from human inaccuracy. For this purpose, the appropriate tools were used to automate and simplify the measurement process. Basically, a mobile platform is used whose pull motors are controlled by a computer. The motors are controlled, and the signals picked up by the microphones recorded, by in-house software specially designed for this task. In this way, the problem of data acquisition for the different measurements is solved, and it is only necessary to apply the required processing for such data. It should be pointed out that the most notable aspect of the measurements obtained is that they give an idea of what a listener would hear at each of the measurement points—in contrast to the first and more usual proposed technique.

The 4100-type *Bruel* and *Kjaer* mannequin receives the signal that a human would perceive in that position with greater accuracy than simply by placing two microphones. To enable accurate measurements, it also includes two $\frac{1}{2}$ in. calibrated Falcon capacitor microphones, located in the hearing channels. Fig. 8 shows the mannequin placed over the mobile platform, which enables monitoring an area of approximately 900 cm^2 at a resolution of 40 μm.

An audio band unit gain preamplifier supplies the capacitor microphones of the mannequin, and acts as an impedance adapter. The signal received by the mannequin's microphones must be filtered before its A/D conversion and storage as data. A band-pass filter through a digital filter with a Analog Devices DSP 2181 was used. The cutoff frequencies of the filters were 230 Hz.

4. Experimental results

Synthesized repetitive noise with harmonics of 15, 20, and 28 Hz, and an 80 Hz single tone were used to test the performance of the multichannel active controller. Up to the first nine harmonics of the signals can be controlled.

4.1. Results at a single point of the space

The measurements obtained in positions close to the error sensors using a 2:2 system with both error sensors at the same z plane will be examined initially. Measurements recorded at the mannequin's right microphone before (solid line) and after (dash line) ANE system operation are shown in Fig. 9(a) for a gain parameter vector $\mathbf{B} = [0, \ldots, 0]^{\mathrm{T}}$ which should cancel a power spectral density of 15 Hz repetitive noise up to the 135 Hz frequency. If the gain parameter vector is $\mathbf{B} = [1\ 0\ 1\ 0\ 1\ 0\ 1\ 0\ 1]^{\mathrm{T}}$, Fig. 9(b) is obtained. In this case, the system cancels ($\beta = 0$) only the

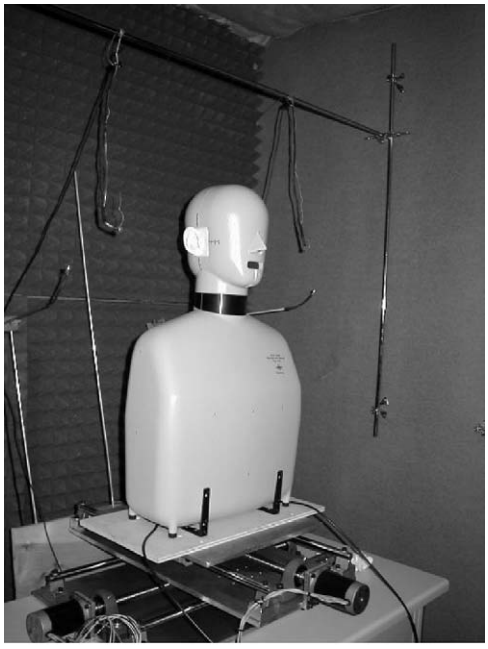

Fig. 8. Mannequin and platform located inside the listening room.

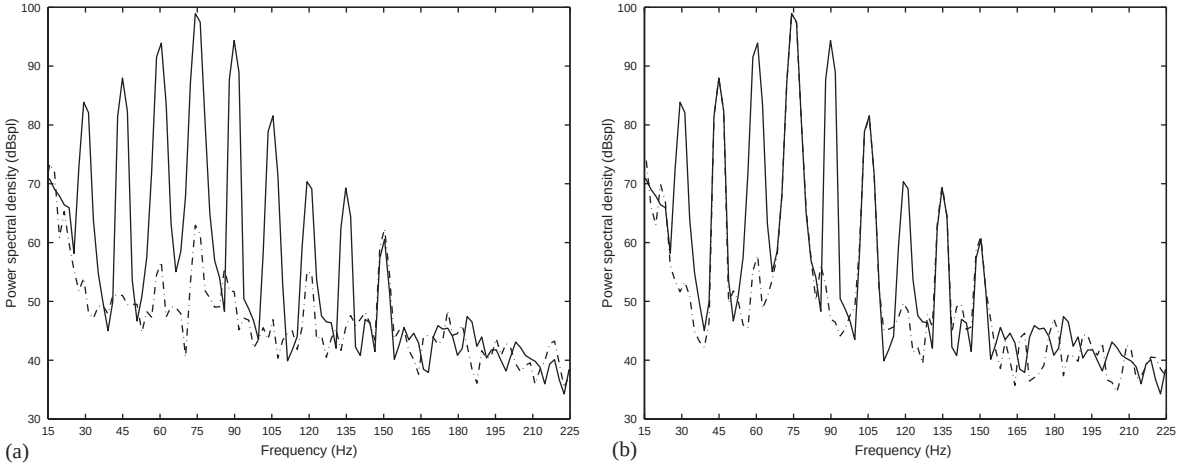

Fig. 9. Power spectral density of synthesized repetitive noise with harmonics of 15 Hz measured at the mannequin's right microphone before active system operation (solid line) and after the active system operation (dashed line) with gain parameter vector: (a) $\mathbf{B} = [0\ 0\ 0\ 0\ 0\ 0\ 0\ 0\ 0]^{\mathrm{T}}$ and (b) $\mathbf{B} = [1\ 0\ 1\ 0\ 1\ 0\ 1\ 0\ 1]^{\mathrm{T}}$.

frequencies: 30, 60, 90, and 120 Hz, the frequency components corresponding to a β parameter equal to 1 remain unchanged.

Fig. 10 illustrates the results obtained using the same reference signal for different gain parameter vectors: Fig. 10(a) with $\mathbf{B} = [0\ 0\ 0\ 0\ 1.5\ 0\ 0\ 0\ 0]^{\mathrm{T}}$ and Fig. 10(b) with

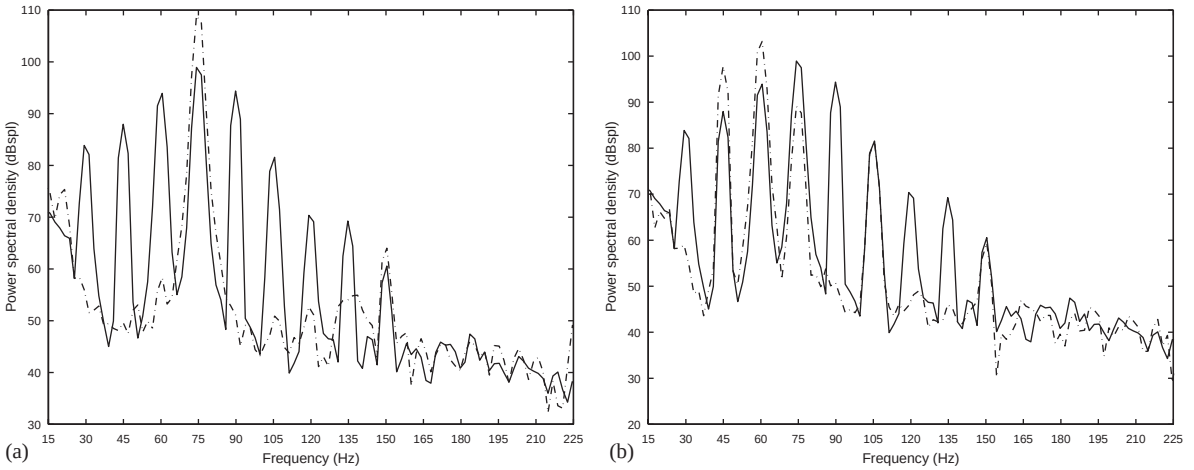

Fig. 10. Power spectral density of synthesized repetitive noise with harmonics of 15 Hz measured at the mannequin's right microphone before the active system operation (solid line) and after the active system operation (dashed line) with gain parameter vector: (a) $\mathbf{B} = [0\ 0\ 0\ 0\ 1.5\ 0\ 0\ 0\ 0]^{\mathrm{T}}$ and (b) $\mathbf{B} = [1\ 0\ 1.5\ 1.5\ 0.5\ 0\ 1\ 0\ 0]^{\mathrm{T}}$.

$\mathbf{B} = [1\ 0\ 1.5\ 1.5\ 0.5\ 0\ 1\ 0\ 0]^{\mathrm{T}}$. As expected, the frequency components corresponding to a β parameter higher than 1, exhibit higher spectrum amplitudes, yet when the β parameter is lower than 1 the spectrum amplitude decreases. It can be seen how the 75 Hz frequency in Fig. 10(a) increases its amplitude, whereas the adjacent frequencies of 60 and 90 Hz are cancelled out. It can be seen in Figs. 9 and 10 that the 150 Hz frequency remains almost unchanged, because the 10th harmonic is not controlled by the active system.

4.2. Zones of equalization

As mentioned earlier, the ability to measure the sound field around the listener head is provided by a mobile platform. The equalization zones can be measured on the plane of the mannequin ears, so that it is possible to record what a listener would hear. A 2:2 system configuration is considered with both error sensors at the same z plane as the one containing the mannequin's ears. Fig. 11 shows the primary noise field for a 80 Hz single tone signal at the listener's ears inside the controlled zone. There is a maximum variation of the primary acoustic field inside the analyzed area of 4.5 dB. It must be noted that the relative head position is shown and the measurement microphone is shown in black. Several experiments were carried out and the equalization areas were measured. Different equalization parameters β were tested. Fig. 12 illustrates the noise reduction levels obtained with the parameter $\beta = 0$ at the mannequin's right microphone (see Fig. 12(a)) and at the mannequin's left microphone (see Fig. 12(b)). Attenuation levels between 26 and 38 dB were achieved and very similar areas were measured with both microphones. The highest attenuation levels belong to the area closest to the $y = 0$ axis and which contains the error sensors of the ANE system. In order to test the noise field levels after the ANE system operation and its relation with the chosen work mode, Fig. 13(a) shows the residual acoustic field levels obtained when $\beta = 0$, Fig. 13(b) when $\beta = 0.3$ and Fig. 13(c) when $\beta = 2$. Results obtained are quite different according to the theory previously developed. Figs. 13(b) and (c) that belong to

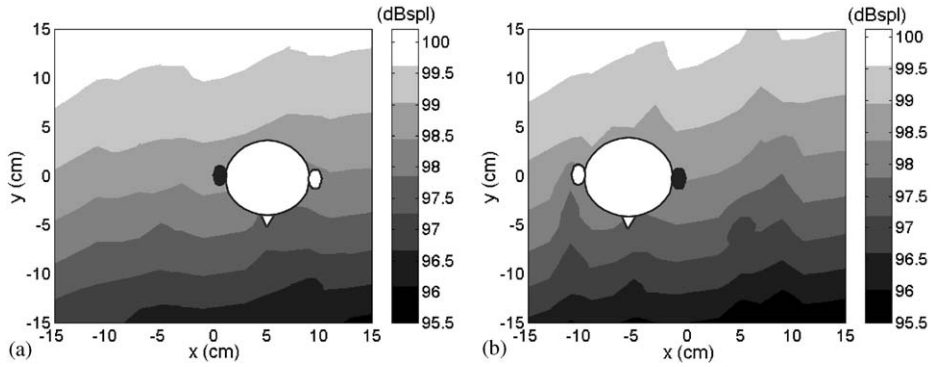

Fig. 11. Sound field for a 80 Hz primary signal. Relative head position is shown. Measurement microphone is colored in black: (a) right microphone and (b) left microphone.

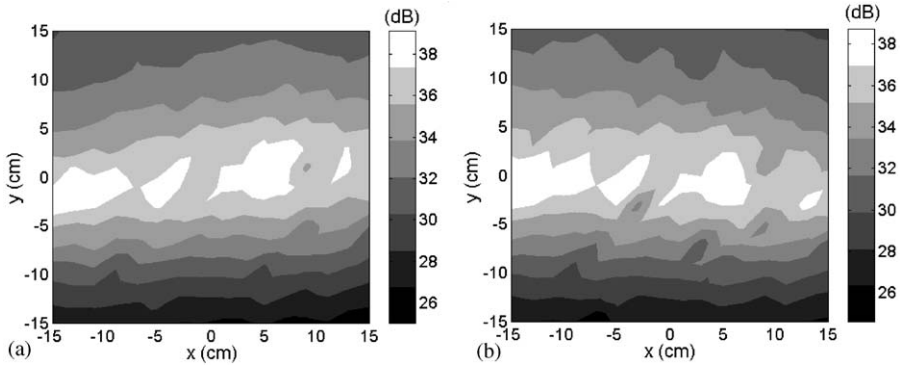

Fig. 12. Attenuation obtained after the ANE system operation in order to cancel 80 Hz single tone: at the mannequin's right microphone (a) and at the mannequin's left microphone (b).

attenuation and amplification work modes, respectively, exhibit maximum variations of around 4 dB between the maximum and minimum noise levels, which are very similar to the variability of the primary noise field measured in Fig. 11(a). The maximum noise level variation achieved when cancellation is desired is around 10 dB, see Fig. 13(a). Fig. 14 illustrates the power spectral density of the 80 Hz single tone at different positions within the controlled area when $\beta = 0.3$. A meaningful amplitude decrease of the 80 Hz tone is observed in all positions.

Now, the results obtained using synthesized repetitive noise with harmonics of 20 Hz will be examined. Fig. 15(a) shows the primary noise field inside the controlled zone measured at the mannequin's left microphone before the ANE system operation. Maximum variation of noise levels is around 3.5 dB. In Fig. 15(b), noise reduction levels are shown for a gain parameter vector $\mathbf{B} = [0, \ldots, 0]^{\mathrm{T}}$. Attenuation levels achieved are lower than those of the previous example due to the complexity of the synthesized repetitive noise field compared with the 80 Hz single tone acoustic field. Maximum noise reduction levels reach 33 dB, whereas the maximum attenuation levels when an 80 Hz single tone was used as primary noise were 38 dB (see Fig. 12). Variability of

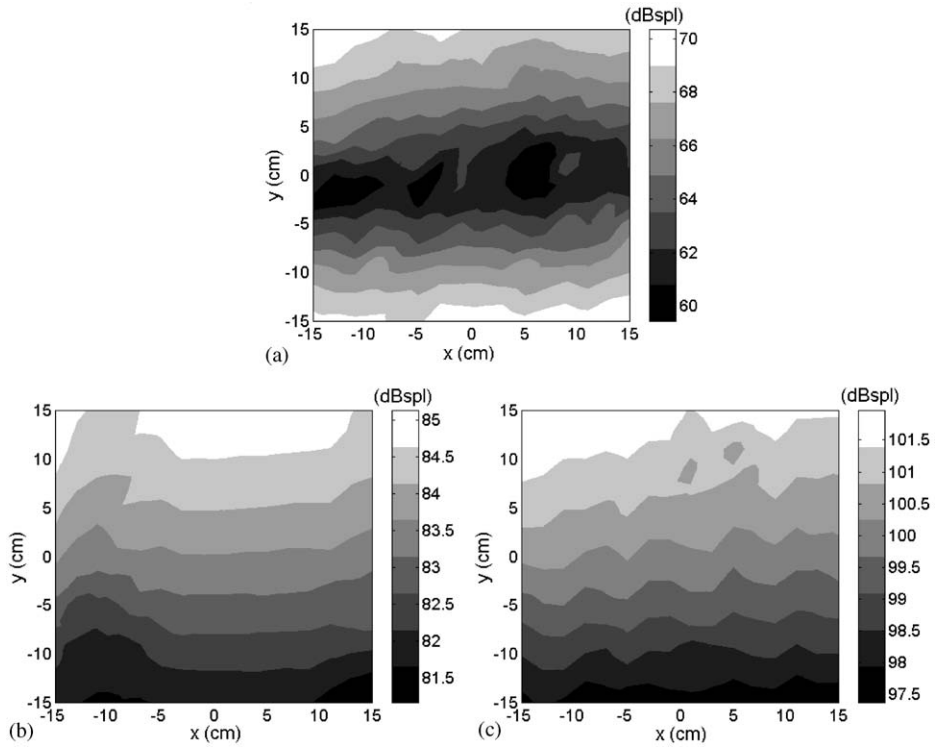

Fig. 13. Residual noise field for 80 Hz single tone measured at the mannequin's right microphone after ANE system operation when: (a) $\beta = 0$, (b) $\beta = 0.3$, and (c) $\beta = 2$.

the residual noise field after active cancellation system operation is higher than in the primary noise field. Maximum variations of around 10 dB between noise levels in the controlled area were recorded, see Fig. 15(c). Therefore, the residual field that results after equalization for gain parameter vectors other than cancellation mode was measured at the mannequin's left microphone. Fig. 16 shows the shape of the acoustic field measured after ANE system operation for a gain parameter vector $\mathbf{B} = [1\ 0\ 1\ 0\ 1\ 0\ 1\ 0\ 1]^{\mathrm{T}}$. Whereas Fig. 17 illustrates the power spectral density at different (x, y) co-ordinates before and after active control system operation. All the positions shown exhibit cancellation only of the even frequency components due to the gain parameter vector setting. However, the 200 Hz frequency is not modified because only up to the first nine harmonics of the signal were controlled.

Finally, in order to test the performance of the system with other transducer configurations, a different arrangement of error sensors was considered. After some laboratory trials, the positioning of the loudspeakers was left unmodified (see Fig. 7) and up to four error sensors were used. Specifically, the tested configurations were (see Fig. 18): 2:2 system (with two error sensors set in an horizontal plane which corresponds to the mannequin's microphone position $z = 0$), 2:4 system (with four error sensors located in the $z = 0$ plane), and 2:4 system, with four error sensors at different z planes (the front error sensors are located at $z = -20$ cm and the rear ones at $z = +20$ cm). Fig. 19 shows the acoustic field for synthesized repetitive noise with harmonics of

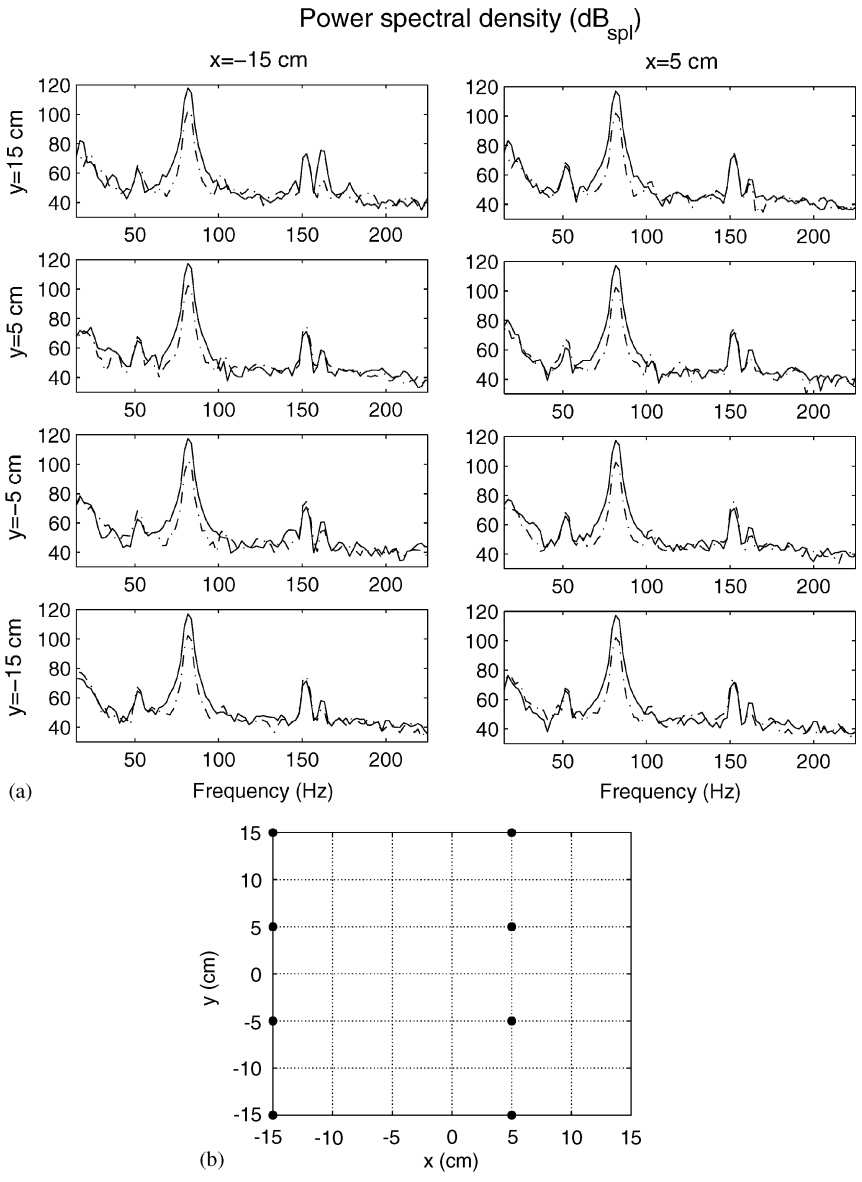

Fig. 14. (a) Power spectral density of the 80 Hz single tone measured at the mannequin's right microphone at different (x, y) co-ordinates when $\beta = 0.3$ before (solid line) and after (dash line) ANE system operation. (b) Sketch of the positions in which power spectral density has been measured.

28 Hz. The residual noise field obtained after ANE operation for a gain parameter vector $\mathbf{B} = [0, \ldots, 0]^{\mathrm{T}}$ and with the error sensors located at the same z plane are shown in Fig. 20(a) (using the 2:2 system configuration) and Fig. 20(b) (2:4 system configuration). Similar results were obtained in both cases with residual noise field levels between 62 and 72 dBspl. In the same way, Figs. 20(c) and (d) show the residual noise field measured in the controlled area on the 2:4 system

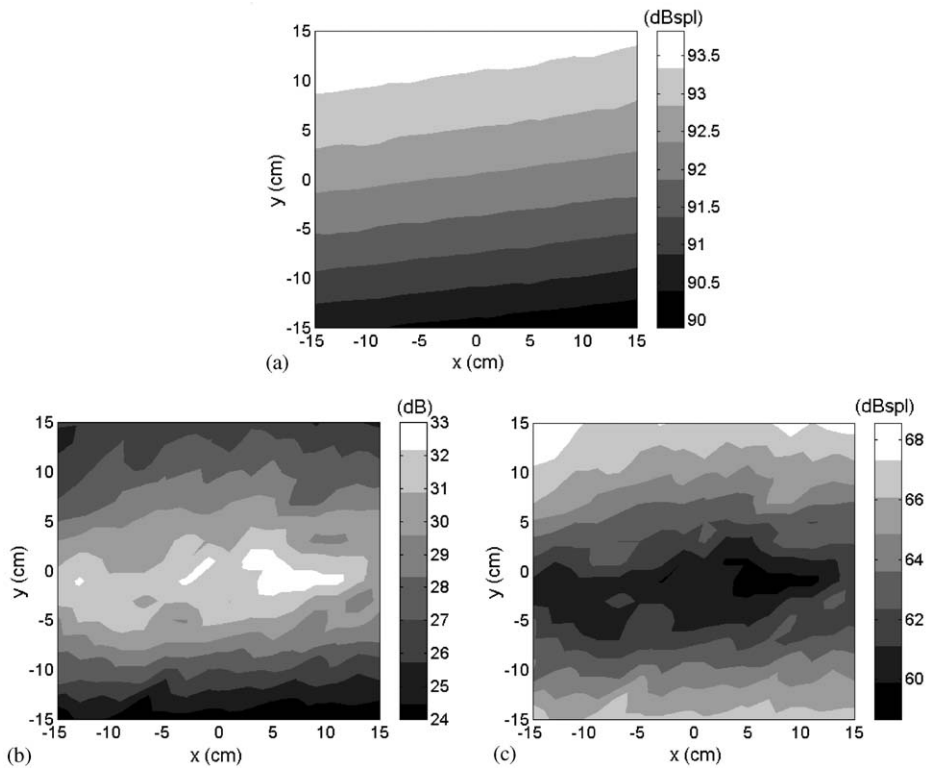

Fig. 15. Synthesized repetitive noise with harmonics of 20 Hz measured at the mannequin's left microphone: (a) before, and (b) and (c) after the ANE system operation for a gain parameter vector $\mathbf{B} = [0, \ldots, 0]^{\mathrm{T}}$ (cancellation mode) ((b) attenuation noise levels achieved and (c) residual noise levels of the acoustic field).

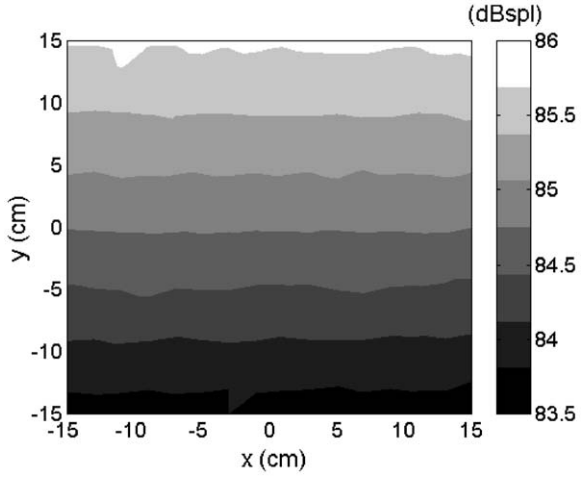

Fig. 16. Noise levels of the residual acoustic field after ANE system operation using synthesized repetitive noise with harmonics of 20 Hz and for the gain parameter vectors $\mathbf{B} = [1\ 0\ 1\ 0\ 1\ 0\ 1\ 0\ 1]^{\mathrm{T}}$. Measured at the mannequin's left microphone.

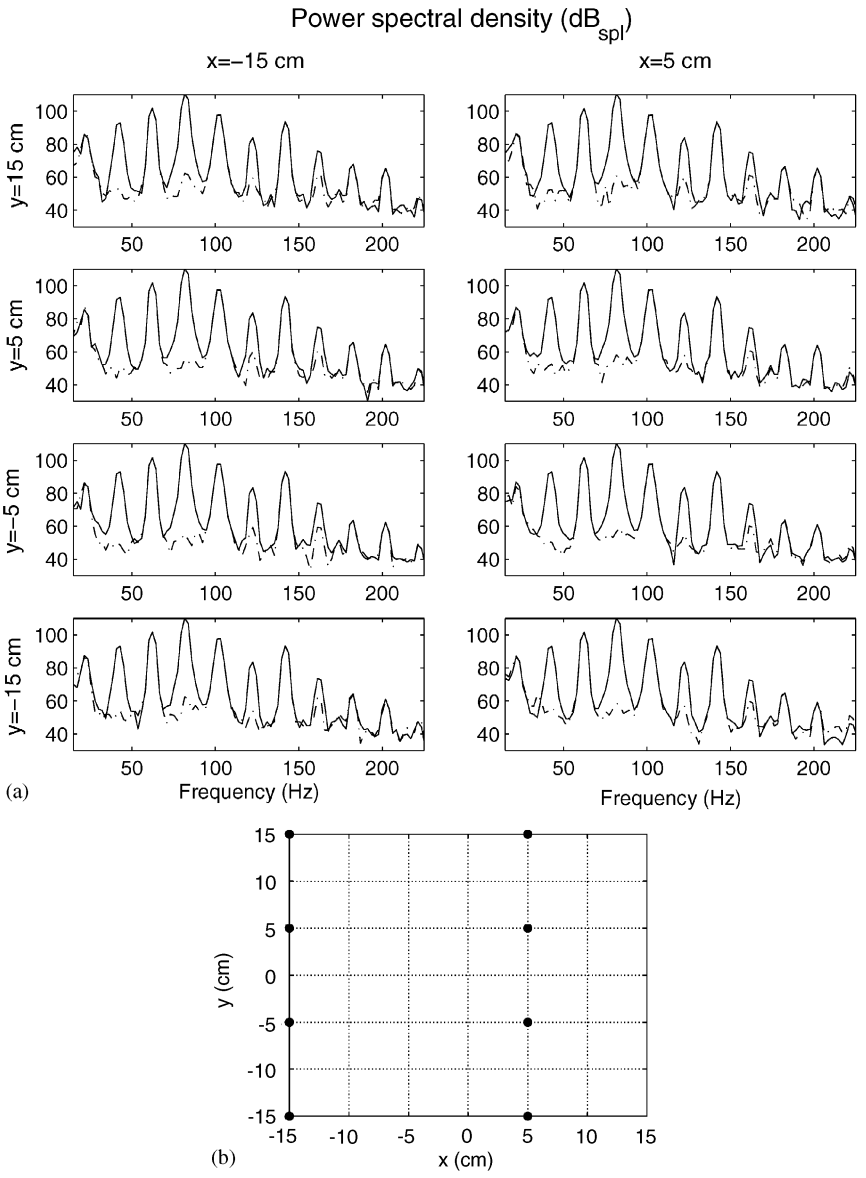

Fig. 17. (a) Power spectral density of synthesized repetitive noise with harmonics of 20 Hz at different (x, y) co-ordinates when $\mathbf{B} = [1\ 0\ 1\ 0\ 1\ 0\ 1\ 0\ 1]^{T}$ before (solid line) and after (dashed line) ANE system operation. Measured at the mannequin's left microphone. (b) Sketch of the positions in which power spectral density has been measured.

configuration with the error sensors at a different z plane (Fig. 20(c) attenuation obtained at the mannequin's right microphone and Fig. 20(d) attenuation obtained at the left microphone). Results demonstrate that the quietest area in Figs. 20(c) and (d) (the darkest zone) is not centred. This is due to the asymmetries of the 2:4 system with error sensors on a different z plane. However, better centred quiet areas were obtained for the other configurations (see Figs. 20(a) and (b)).

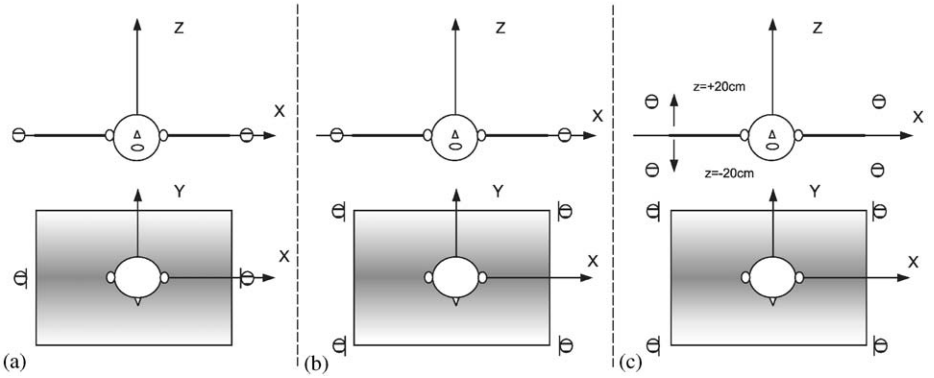

Fig. 18. Front view and upper view for different error sensor configuration: (a) 2:2 system with two error sensors at the same z plane, (b) 2:4 system with four error sensors at the same z plane, and (c) 2:4 system, with four error sensors at different z plane.

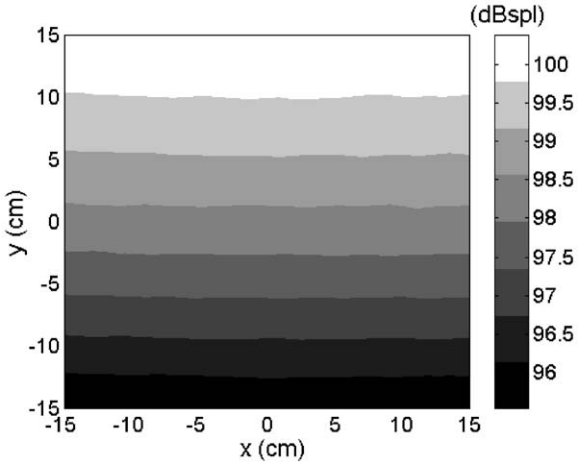

Fig. 19. Noise field for synthesized repetitive noise with harmonics of 28 Hz before ANE system operation. Measurements at the mannequin's right microphone.

5. Conclusions

This paper describes the implementation of a real-time multichannel system for the active equalization of noise in enclosures.

The equalization algorithm developed in the multichannel controller is described initially in its simplest version, which is the single frequency ANE (SFANE), upto the more advanced multichannel multifrequency version as an extension of the SFANE algorithm.

The prototype is described in detail with an analysis of the acoustic characteristics of the room, which was modified to achieved suitable reverberation characteristics. The different acoustic and electrical components of the system are described, as well as the measurement system, which basically consists of a head and torso simulator and a linear measurement platform.

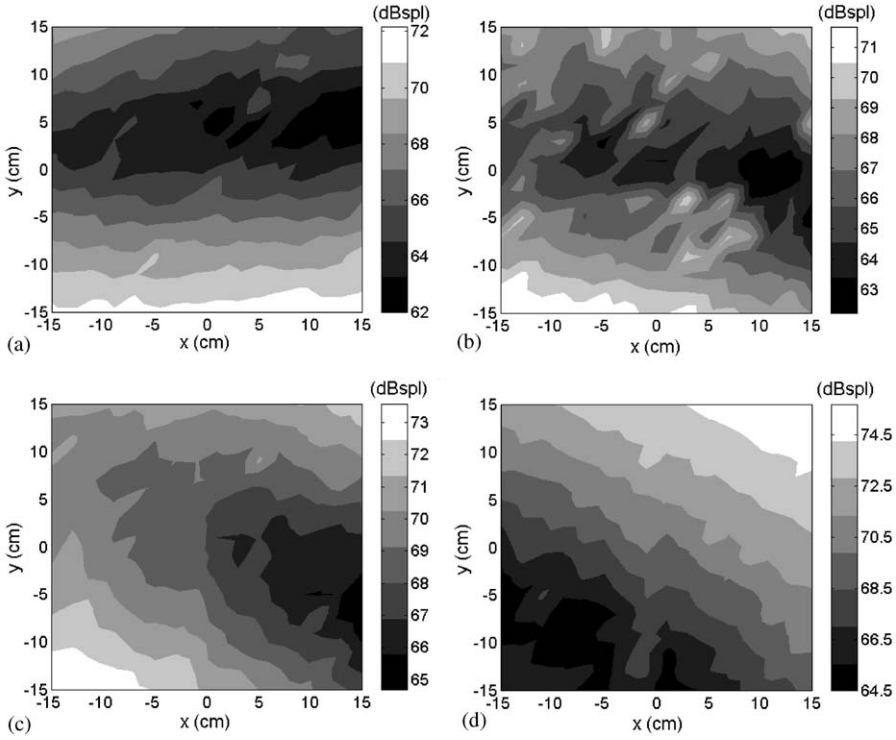

Fig. 20. Residual noise field after the ANE system operation using synthesized repetitive noise with harmonics of 28 Hz for a gain parameter vector $\mathbf{B} = [0, \ldots, 0]^{\mathrm{T}}$ using: (a) a 2:2 system configuration, (b) a 2:4 system configuration and the error sensors located on the same z plane, and (c) and (d) 2:4 system configuration and error sensors located on different z plane ($z = 20$ and -20 cm). Measurements: (a)–(c) at the mannequin's right microphone and (d) at the mannequin's left microphone.

To evaluate the performance of the system, several measurements were conducted with different transducer configurations and parameter settings. Firstly, measurements were taken at single points to test the effectiveness of the equalizers when individually controlling the reference signals. However, in practice, the most meaningful measurements were the equalization areas. These were measured by moving the mannequin in an area of 900 cm^2, and binaurally recording the sound signals every 3 cm around the mannequin's initial position before, and after, the equalization. This method of measuring equalization zones allows determination of what a listener would hear at each point of the controlled area with, and without, control. The shape of the obtained residual field changes depending on the gain parameter vectors applied, and on the nature of the primary signal. It is a fact that in a standing single frequency field, pressure minima are very sharp and maxima are flat [23]. Therefore, the cancelling wave should exhibit sharp pressure minima and flat maxima in order to cancel the primary signal. That is why in the case of cancellation (gain parameters equal to zero), a non-homogeneous residual acoustic field is obtained in the controlled area. Specifically, the variability of the residual field reaches up to 10 dB for the 80 Hz single tone primary signal, and is symmetrically distributed with respect to the y-axis that contains the error sensors ($y = 0$), thus increasing noise levels as distances increase (see Figs. 13(a) and 15(c)).

Similar conclusions are obtained for more complex field, but noise reduction levels decrease with the complexity of the primary noise field (compare Figs. 12(b) and 15(b)). However, if equalization is desired, a more uniform acoustic field is necessary, because the generated controlling waves has only to modified the primary waves slightly. The variability of the residual field when a total cancellation of the primary noise field is not desired (gain parameters different to zero) is very similar to the variability of the primary noise field (around 3.5 dB), with an increase of noise levels in the area closest to the rear acoustic foam wall (see the comparison between Figs. 15(a) and 16(a)).

The position of loudspeakers and error sensors has been shown to be important to achieve a certain acoustic sensation in the controlled area. Among the different transducer configurations tested, the loudspeakers are best placed facing the mannequin on a z plane, close to the plane which contains the mannequin's ears, with the secondary loudspeakers on each side of the primary speaker. The combination of two microphones placed in the $y = 0$ axis provided good results (which means higher attenuation of noise levels in the cancellation mode) and a simpler implementation compared with the other arrangements tested (since less error sensors provide a reduction in computational complexity and electroacoustic components). A similar study was applied for the ANC system reported in Ref. [24]. The shape of the controlled area was not as sensitive as the location of other error sensors relative the loudspeakers placement. See Fig. 20 for an example.

Finally, the experimental results confirmed the ability of the system to control independently frequencies in the area analyzed, not only to reduce the existing acoustic power, but to configure the sound field perceived in the appropriate form and create a specific acoustic sensation. However, the difficulty lies in deciding which is the acoustic sensation that best fits each listener preference for each particular application, since subjective considerations intervene and they, in turn, require subjective analysis [5,25,26].

Acknowledgements

This work was partially supported by: CICYT Projects TIC2000-1683-C03 and TIC99-0444-C02, and Catedra Motorola.

References

[1] J. Feng, W. Gan, Adaptive active noise equalizer, *Electronics Letters* 33 (18) (1997) 1518–1519.
[2] J. Feng, W. Gan, Broadband active noise compressor, *IEEE Signal Processing Letters* 5 (1) (1998) 11–14.
[3] S. Kuo, D. Morgan, *Active Noise Control Systems*, Wiley, New York, 1996.
[4] M. de Diego, A. Gonzalez, G. Pinero, M. Ferrer, J.J. Garcia-Bonito, Subjective evaluation of actively controlled interior car noise, *Proceedings of the International Conference on Acoustics, Speech and Signal Processing* (*ICASSP*), May 2001.
[5] A. Gonzalez, M. Ferrer, M. de Diego, G. Piñero, J.J. Garcia-Bonito, Sound quality of low-frequency and car engine noises after active noise control, *Journal of Sound and Vibration* 265 (3) (2003) 663–679.
[6] B. Widrow, J.R. Glover, J.M. McCool, J. Kaunitz, C.S. Williams, R.H. Hearn, J.R. Zeidler, E. Dong, R.C. Goodlin, Adaptive noise cancelling: principles and applications, *Proceedings of the IEEE* 63 (12) (1975) 1692–1716.

[7] J. Glover, Adaptive noise cancelling applied to sinusoidal interferences, *IEEE Transactions on Acoustics Speech and Signal Processing* 25 (6) (1977) 484–491.
[8] S.J. Elliott, P. Darlington, Adaptive cancellation of periodic, synchronously sampled interference, *IEEE Transactions on Acoustics, Speech and Signal Processing* 33 (3) (1985) 715–717.
[9] B. Widrow, S.D. Stearns, *Adaptive Signal Processing*, Prentice-Hall, Englewood Cliffs, NJ, 1985.
[10] S.J. Elliott, I.M. Stothers, P.A. Nelson, A multiple error lms algorithm and its application to the active control of sound and vibration, *IEEE Transactions on Acoustics, Speech and Signal Processing* 35 (10) (1987) 1423–1434.
[11] M. de Diego, A. Gonzalez, C. Garcia, On the performance of a local active noise control system, *Proceedings of the International Conference on Acoustics*, *Speech and Signal Processing* (*ICASSP*), Vol. 2, Arizona, March 1999, pp. 885–888.
[12] D. Morgan, C. Sanford, A control theory approach to the stability and transient analysis of the filtered-x lms adaptive notch filter, *IEEE Transactions on Signal Processing* 40 (9) (1992) 2341–2346.
[13] X. Kong, S. Kuo, Study of causality constraint on feedforward active noise control systems, *IEEE Transactions on Circuits and Systems-II: Analog and Digital Signal Processing* 46 (2) (1999) 183–186.
[14] S.M. Kuo, M.J. Ji, X.H. Jiang, Development and experiment of narrowband active noise equalizer, *Noise Control Engineering Journal* 41 (3) (1993) 281–288.
[15] M.J. Ji, S.M. Kuo, An active harmonic noise equalizer, *Proceedings of the International Conference on Acoustics*, *Speech and Signal Processing* (*ICASSP*), Vol. 1, Minneapolis, MN, April 1993, pp. 189–192.
[16] S.M. Kuo, M.J. Ji, Development and analysis of an adaptive noise equalizer, *IEEE Transactions on Speech and Audio Processing* 3 (3) (1995) 217–222.
[17] B. Widrow, M.E. Hoff, Adaptive switching circuits, *Proceedings IRE WESCON Convention Record*, Part 4 (Session 16) (1960) 96–104.
[18] S.M. Kuo, Multiple-channel adaptive noise equalizers, *Proceedings of the 29th Asilomar Conference on Signals, Systems, and Computers*, Vol. 1, Pacific Grove, CA, October 1996, pp. 1250–1254.
[19] P.A. Nelson, S.J. Elliott, *Active Control of Sound*, Academic Press, New York, 1992.
[20] A. Gonzalez, Active Control of Noise using Adaptive Signal Processing, PhD Thesis, Technical University of Valencia, Spain, 1997 (in Spanish).
[21] M. de Diego, A. Gonzalez, C. Garcia, M. Ferrer, Some practical insights in multichannel active noise control equalization, *Proceedings of the International Conference on Acoustics*, *Speech and Signal Processing* (*ICASSP*), Vol. 2, Istanbul, May 2000, pp. 837–840.
[22] M. de Diego, Multichannel Adaptive Equalization for Active Control of Interior Noise, PhD Thesis, Technical University of Valencia, Spain, 2003 (in Spanish).
[23] H. Kuttruf, *Room Acoustics*, 3rd Edition, Elsevier Science Publisher Ltd., New York, 1991.
[24] M. de Diego, A. Gonzalez, Performance evaluation of multichannel adaptive algorithms for local active noise control, *Journal of Sound and Vibration* 244 (4) (2001) 615–634.
[25] U. Widmann, Aurally adequate evaluation of sounds, Plenary lecture. *Euronoise-98*, Munich, 1998, pp. 1–18.
[26] A. Gonzalez, M. Ferrer, M. de Diego, G. Piñero, Subjective considerations in multichannel active noise control equalization of repetitive noise, *Proceedings of the ACTIVE 2002*, Vol. 1, Southampton, July 2002, pp. 387–397.